


## RESEARCH ARTICLE

# Altered Spinal Cord Functional Connectivity Associated with Parkinson's Disease Progression

Caroline Landelle, PhD,<sup>1\*</sup>  Linda Solstrand Dahlberg, PhD,<sup>1</sup> Ovidiu Lungu, PhD,<sup>1</sup> Bratislav Misic, PhD,<sup>1</sup> Benjamin De Leener, PhD,<sup>2,3</sup> and Julien Doyon, PhD<sup>1</sup>

<sup>1</sup>Department of Neurology and Neurosurgery, McConnell Brain Imaging Centre, Montreal Neurological Institute, McGill University, Montreal, Quebec, Canada

<sup>2</sup>Department of Computer Engineering and Software Engineering, Polytechnique Montreal, Montreal, Quebec, Canada

<sup>3</sup>CHU Sainte-Justine Research Centre, Montreal, Quebec, Canada

**ABSTRACT: Background:** Parkinson's disease (PD) has traditionally been viewed as an  $\alpha$ -synucleinopathy brain pathology. Yet evidence based on postmortem human and animal experimental models indicates that the spinal cord may also be affected.

**Objective:** Functional magnetic resonance imaging (fMRI) seems to be a promising candidate to better characterize spinal cord functional organization in PD patients.

**Methods:** Resting-state spinal fMRI was performed in 70 PD patients and 24 age-matched healthy controls, the patients being divided into three groups based on their motor symptom severity: PD<sub>low</sub> (n = 24), PD<sub>med</sub> (n = 22), and PD<sub>adv</sub> (n = 24) groups. A combination of independent component analysis (ICA) and a seed-based approach was applied.

**Results:** When pooling all participants, the ICA revealed distinct ventral and dorsal components distributed along the rostro-caudal axis. This organization was highly reproducible within subgroups of patients and controls. PD severity, assessed by Unified Parkinson's Disease Rating Scale (UPDRS) scores, was associated with a

decrease in spinal functional connectivity (FC). Notably, we observed a reduced intersegmental correlation in PD as compared to controls, the latter being negatively associated with patients' upper-limb UPDRS scores ( $P = 0.0085$ ). This negative association between FC and upper-limb UPDRS scores was significant between adjacent C4–C5 ( $P = 0.015$ ) and C5–C6 ( $P = 0.20$ ) cervical segments, levels associated with upper-limb functions.

**Conclusions:** The present study provides the first evidence of spinal cord FC changes in PD and opens new avenues for the effective diagnosis and therapeutic strategies in PD. This underscores how spinal cord fMRI can serve as a powerful tool to characterize, in vivo, spinal circuits for a variety of neurological diseases. © 2023 The Authors. *Movement Disorders* published by Wiley Periodicals LLC on behalf of International Parkinson and Movement Disorder Society.

**Key Words:** Parkinson's disease; functional magnetic resonance imaging; spinal cord; resting state; spinal networks

Parkinson's disease is associated with the neurodegeneration of dopaminergic neurons in the substantia nigra par compacta and with the presence of abnormal aggregation of  $\alpha$ -synuclein outside the

substantia nigra called Lewy bodies.<sup>1,2</sup> The popular Braak and Tredici model<sup>3,4</sup> hypothesizes that Lewy body formation spreads in a topographically predictable pattern from the olfactory bulb and/or peripheral

This is an open access article under the terms of the [Creative Commons Attribution-NonCommercial-NoDerivs](https://creativecommons.org/licenses/by-nc-nd/4.0/) License, which permits use and distribution in any medium, provided the original work is properly cited, the use is non-commercial and no modifications or adaptations are made.

\*Correspondence to: Dr. Caroline Landelle, Department of Neurology and Neurosurgery, McConnell Brain Imaging Center, Montreal Neurological Institute, McGill University, 3801 University Street, Montreal, Quebec H3A 2B4, Canada; E-mail: [caroline.landelle@mcgill.ca](mailto:caroline.landelle@mcgill.ca)

**Relevant conflicts of interest/financial disclosures:** The authors declare that they have no known competing financial interests or

personal relationships that could have appeared to influence the work reported in this paper.

**Funding agencies:** This work was supported by Fondation Courtois and the Natural Sciences and Engineering Research Council of Canada (NSERC) (RGPIN-248074). C.L. was supported by the Fonds de Recherche du Québec—Santé (FRQ-S).

**Received:** 17 November 2022; **Revised:** 13 January 2023; **Accepted:** 30 January 2023

Published online in Wiley Online Library ([wileyonlinelibrary.com](https://www.wileyonlinelibrary.com)). DOI: 10.1002/mds.29354

and enteric nervous system into the brainstem followed by the presence of such neuropathological markers in subcortical and cortical areas.<sup>3-5</sup>

Although PD has been considered to be mainly a brain disease, accumulated evidence on postmortem humans and animal experimental models indicates that the spinal cord may also be affected by  $\alpha$ -synucleinopathy.<sup>3,6,7</sup> For instance, human postmortem studies have reported that the spinal cord  $\alpha$ -synuclein agglomeration was associated with aging,<sup>8,9</sup> clinical assessments of parkinsonism or PD diagnosis,<sup>3,8,10-12</sup> and  $\alpha$ -synuclein agglomeration at the brain level.<sup>8,9,11</sup> These lesions were found more frequently in the lower brainstem, especially in the motor nucleus of the vagus nerve than in the spinal cord, thus suggesting that the disease process starts in the lower brainstem and then descends toward the spinal cord.<sup>3,9,11,13</sup> In addition, neuronal death was found in both the ventral (motoneurons) and dorsal (somatosensory neurons) parts of PD patients' spinal cord.<sup>3,14</sup>

Based on evidence gathered so far, it appears that a deeper characterization of the functional alterations observed in the spinal cord is needed to achieve a better characterization of the PD neuropathological mechanisms. To achieve this goal, we propose to use spinal resting-state functional magnetic resonance imaging (rsfMRI) techniques.<sup>15-19</sup> Although this imaging approach remains challenging, recent advances have overcome some of its key technical difficulties and rendered it an accessible tool that can be used noninvasively to investigate the functional organization of the spinal cord, *in vivo*.<sup>20-22</sup> Similar to that in the brain, spinal rsfMRI reveals a functional organization in circuits consistent with that observed from neurophysiological investigations,<sup>21</sup> such as its functional lateralization, rostro-caudal segmental segregation, and the separation between motor and sensory pathways.<sup>15,17,18,23</sup>

Yet no previous study has used rsfMRI to evaluate PD-related functional changes in the spinal cord. In response to this knowledge gap, we employed spinal cord rsfMRI in a sample of 94 PD patients and healthy controls (HC) to characterize the disease-related differences in resting-state functional connectivity (FC). In particular, we assessed the level of synchronization of the cervical spinal cord activity at rest, as well as that of the intra- and intersegmental FC in both PD patients, who underwent a clinical evaluation of their motor symptoms before the MRI scan, and in a HC group. We hypothesized that (1) similar to the brain, the cervical spinal cord resting-state activity is organized in independent networks whose FC is altered by the disease; and (2) such a change in FC network segregation in PD patients will be proportional to the severity of the motor symptoms, therefore reflecting disease progression.

## Patients and Methods

### Participants

Seventy-seven patients with idiopathic ("of unknown origins") PD (54 men; age,  $64.55 \pm 9.0$  [40–83] years) and 24 matched HC participants (9 men; age,  $64.33 \pm 9.3$  [39–83] years) with no history of neurological diseases or motor disorder were recruited in the present study. All participants gave their written consent in accordance with the Helsinki Declaration, and the experiment was approved by the local ethics committee (MUCH REB 2019-4626). The data from 7 participants were excluded from the final analyses due to poor quality of the anatomical ( $n = 1$ ) or fMRI images (ie, low temporal signal-to-noise ratio,  $n = 4$ ) and to large amounts of motion ( $n = 2$ , details in Supporting Data). Thus, the final sample consisted of 70 PD patients (50 men;  $64.89 \pm 9.0$  [40–83] years) and 24 HCs (9 men,  $64.33 \pm 9.3$  [39–83] years). All participants were recruited through the Clinical, Biospecimen, Imaging and Genetic (C-BIG) repository and underwent clinical interviews and neurological examinations, including the Montreal Cognitive Assessment and UPDRS (Unified Parkinson's Disease Rating Scale, 2003),<sup>24</sup> as part of their inclusion (see details in Supplementary Table S1). PD patients were subsequently divided into three nearly equal groups based on the severity of motor symptoms (low, medium, and advanced) measured using the UPDRS, Part III, score: PD<sub>low</sub> group ( $n = 24$ , 14 men,  $60.96 \pm 9.4$  [40–82] years, UDPRS scores: [0–20]), PD<sub>med</sub> group ( $n = 22$ , 18 men,  $64.45 \pm 6.7$  [48–74] years, UDPRS scores: [20–30]), and PD<sub>adv</sub> group ( $n = 24$ , 18 men,  $69.21 \pm 8.6$  [48–83] years, UDPRS scores: [30–60]). Dividing PD patients into three groups will allow us to perform group comparisons with HCs based on disease progression.

### Data Acquisition

MRI data were acquired using a 3-T MRI scanner (Magnetom-Prisma, Siemens, Erlangen, Germany) at The Neuro (Montreal Neurological Institute) using a 64-channel phase-array head coil (one to seven elements active) and a neck coil (one to two elements active). Participants were placed in the scanner in supine position, while wearing Neck and Brachial Plaxus SatPads. These pads contain a nonprotonated perfluorocarbon liquid that is used as a fat-saturation and stabilization device for MRI, with the potential to improve local magnetic field homogeneity and provide in higher-quality images.<sup>25</sup> Throughout the scanning session, the participants were instructed to minimize their motion, to relax, and to try to swallow as gently as possible.

Anatomical images were first acquired using a high-resolution T1-weighted sequence that covered the whole brain and the cervical spinal cord up to T1 vertebrae in most participants (MPRAGE [magnetization prepared rapid gradient echo] sequence, GRAPPA [generalized autocalibrating partial parallel acquisition] iPAT [integrated parallel acquisition techniques] acceleration factor = 2, interleaved sagittal acquisition, Repetition time (TR)/ Inversion time (TI)/ Echo Time (TE) = 2300/925/3.3 ms, voxel size =  $1.3 \times 1.3 \times 1.3 \text{ mm}^3$ , Field of view (FOV) =  $228 \times 364 \times 375 \text{ mm}^3$  [left posterior inferior] (LPI) orientation], flip angle =  $9^\circ$ ). Blood-oxygen-level-dependent images using a gradient-echo EPI (echo planar imaging) sequence were subsequently acquired with a multiband sequence covering the brain and cervical spinal cord (transversal acquisition, perpendicular to the spinal cord; axial plane voxel size =  $1.6 \times 1.6 \text{ mm}^2$ ; axial FOV =  $192 \times 192 \text{ mm}^2$ ; slice thickness = 4 mm; number of slices = 69; GRAPPA iPAT acceleration factor = 3; TR = 1550 ms; TE = 23 ms; flip angle =  $70^\circ$ ; number of volumes = 265; duration = 7:05 min). The EPI slices were positioned using the high-resolution T1w image so that the FOV is positioned parallel to the spinal cord, and the shim volume was manually set to focus on the spinal cord, as described in the generic acquisition protocol.<sup>26</sup> During fMRI acquisition, physiological recordings were acquired using a pulse sensor and a respiration belt.

### Data Preprocessing

The functional and structural images of the spinal cord were preprocessed using the Spinal Cord Toolbox (version 5.0)<sup>27</sup> and the Oxford Center for fMRI of the Software Library (FSL, version 5.0). The preprocessing steps consisted of (1) slice timing correction, (2) motion correction, (3) segmentation of functional and structural images, and (4) coregistration of functional image to T1w image and then to PAM50 template.<sup>27</sup> Then, for each individual, we accounted for the physiological and other noise sources by modeling nuisance noises present in the cerebrospinal fluid using the Tapas PhysiO toolbox.<sup>28</sup> Details on fMRI preprocessing and processing are provided in Supporting Data (Figs. S1 and S2).

### Independent Component Analysis

#### CanICA Approach

Independent component analysis (ICA) is a data-driven method used to extract statistically independent spatially clustered activity patterns that are embedded in the data. A group-level ICA analysis was performed on the whole sample of participants ( $n = 94$ ) using the CanICA method<sup>29</sup> implemented in the Nilearn toolbox, a Python package that uses the scikit-learn library.<sup>30</sup> The aim of this analysis (details in Supporting Data) was to identify spinal cord networks that overlap with

the location of the known segmental levels<sup>31</sup> and those recently characterized in a dynamic FC study involving C5–C8 segments.<sup>17</sup> The independent components (ICs) obtained were  $z$ -scored and thresholded at  $z = 4$  for further analyses and for illustration purposes.

#### Spatial Distribution of ICs

Each  $z$ -scored IC was named based on their rostro-caudal position (ie, closest segmental level) and on their axial distribution (ventral, dorsal, left, right, or central if the IC was found in the middle of the spine, see Supporting Material).

#### Group Similarity

To investigate whether the ICs were stable across the different subgroups (ie, HC, PD<sub>low</sub>, PD<sub>med</sub>, and PD<sub>adv</sub>), four separate CanICA analyses were conducted. The CanICA procedure was the same as the one applied to the whole sample regardless of subgroup membership. Then, group similarity was accessed using the Dice coefficient calculation (ie, twice the overlapping voxels between the ICA map of the population and the subgroup divided by the total number of voxels in both maps) for each possible pairwise IC comparison. Four matrices of Dice coefficient ( $15 \times 15$ ) were constructed to assess IC similarity between each subgroup and IC from the whole population.

### Seed-to-Seed Analysis

#### Regions of interest

The seeds or regions of interest (ROIs) used in FC analysis were selected based on the ICs obtained from the whole sample ICA (Fig. S2A). Therefore, each of the IC maps was combined with a binary mask specific to each of the four horns of the GM atlas (left dorsal: LD, left ventral: LV, right dorsal: RD, right ventral: RV), with the resulting overlap between the IC map and a particular spinal horn used as an ROI. Using this approach, we were able to create 32 seeds.

#### Signal extraction and FC matrices

At the individual level, the time series within each of the 32 ROIs was detrended and  $z$ -scored (Fig. S2B). Fisher's  $r$ -to- $z$  Pearson's correlation coefficients ( $z$ Corr) were computed between all ROI pairs, and the average group matrices were computed. To examine intragroup FC between ROIs, statistical tests assessed whether the  $z$ Corr were significantly different from 0, and the results were considered significant if they survived the false discovery rate (FDR) method for multiple comparison ( $P < 0.05$ ).  $z$ Corr between ROIs localized in the same segmental level were considered as intrasegmental FC measures, whereas  $z$ Corr between ROIs localized in

the different segmental levels were considered as inter-segmental FC measures (Fig. S2C).

### Inter- and intrasegmental FC

The  $z$ Corr between ROIs at different segmental levels were used to investigate intersegmental connectivity. First, we investigated the differences in global inter-segmental FC between groups. Second, we evaluated the effect of rostro-caudal distance (ie, the effect of distance, in millimeters, between segments) in the interaction with the group variable. Third, we focused our analyses on the FC between two adjacent spinal segments. Finally, to investigate intrasegmental FC we computed the  $z$ Corr between pairs of ROIs that were localized within the same segmental level.

Details of the seed-to-seed analyses are provided in Supporting Data.

### Statistical Analyses

Linear mixed models and linear regression models were carried out using the R package lme4 in R programming language. All statistical models included the age of the participants as a fixed effect to control for its potential effect on the dependent variables, even though we were not interested in its explanatory role. The effect of sex factor and disease lateralization was also tested (see the Supplementary Material).

Models were fitted to data using the maximum likelihood approach as implemented in the R lmerTest package. The Satterthwaite's method was applied to models, without interaction terms, for the estimation of the degree of freedom,  $t$  statistics, and associated  $P$ -values. Wald  $\chi^2$  tests were used to estimate statistical parameters for models with interaction terms.

The statistical significance level was set to  $P < 0.05$ , with all  $P$ -values being FDR corrected for multiple comparisons when necessary.

To investigate the contribution of motor symptom severity to cervical spinal cord FC, we calculated the sum of the UPDRSIII scores of the upper or lower limbs (ie, UPDRSIII items related to the upper or lower limbs, respectively), and we then performed regressions between this variable and other FC measures.

## Results

### Independent Component Analysis

Group-ICA analysis on the entire sample ( $n = 94$ ) resulted in 15 spinal ICs spatially segregated with limited rostro-caudal extents (Fig. 1); 13 of 15 components strongly matched the known spinal levels between C1 and C6. The spatial distribution in the axial plane was bilateral in 13 of 15 components (ie, overlapped right and left sides) and strongly confined to the ventral or dorsal part of the spinal cord (Fig. 1; Supporting Data for details). ICA performed within each group of participants (ie, HC, PD<sub>low</sub>, PD<sub>med</sub>, and PD<sub>adv</sub>) revealed a high spatial similarity between the ICs obtained in each group (Supporting Data Fig. S3).

The correlation matrices provided an overview of the FC between distant segments (intersegmental FC) and of the same segmental levels (intrasegmental FC) in each group. In the HC group, we observed significant positive correlations between short-distance ROIs that tended to decrease with distance. Negative correlations between long-distance segments were also observed (Fig. 2). These findings were similar in the PD groups; however, the number of significant correlations decreased for the more affected PD groups (total number of significant correlations for HC: 84, PD<sub>low</sub>:

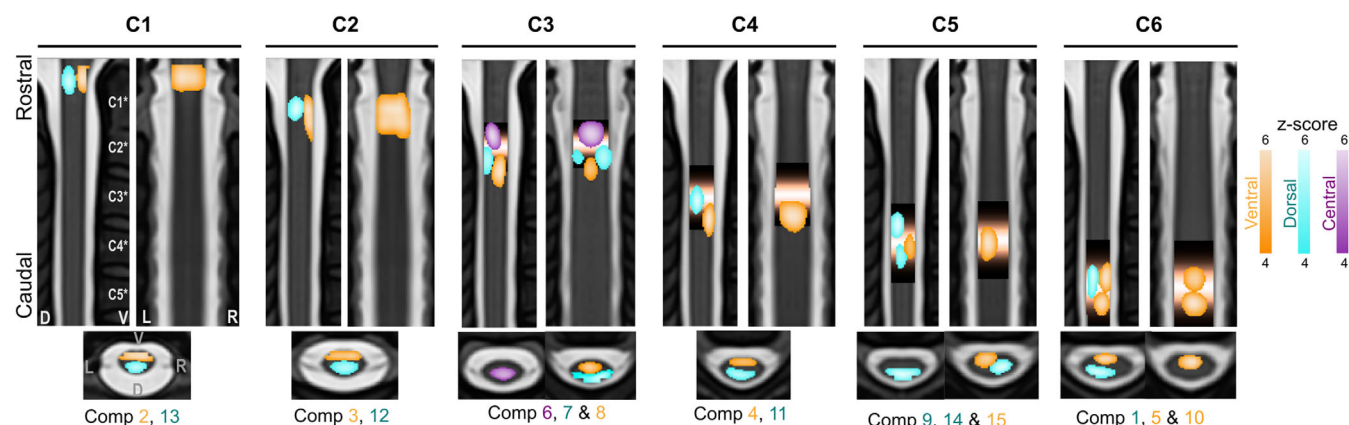


**FIG. 1.** Independent component analyses (ICA). ICA spatial maps are presented in sagittal, coronal, and axial views. Thresholded ICA maps ( $z > 4$ ) are displayed on PAM50 template and superposed on the probabilistic maps of the corresponding spinal level (for levels C3–C6). Blue: dorsal components, red: ventral components, violet: central component. Component numbers are indicated at the bottom. L, left; R, right; D, dorsal; V, ventral. [Color figure can be viewed at [wileyonlinelibrary.com](https://onlinelibrary.wiley.com/terms-and-conditions)]



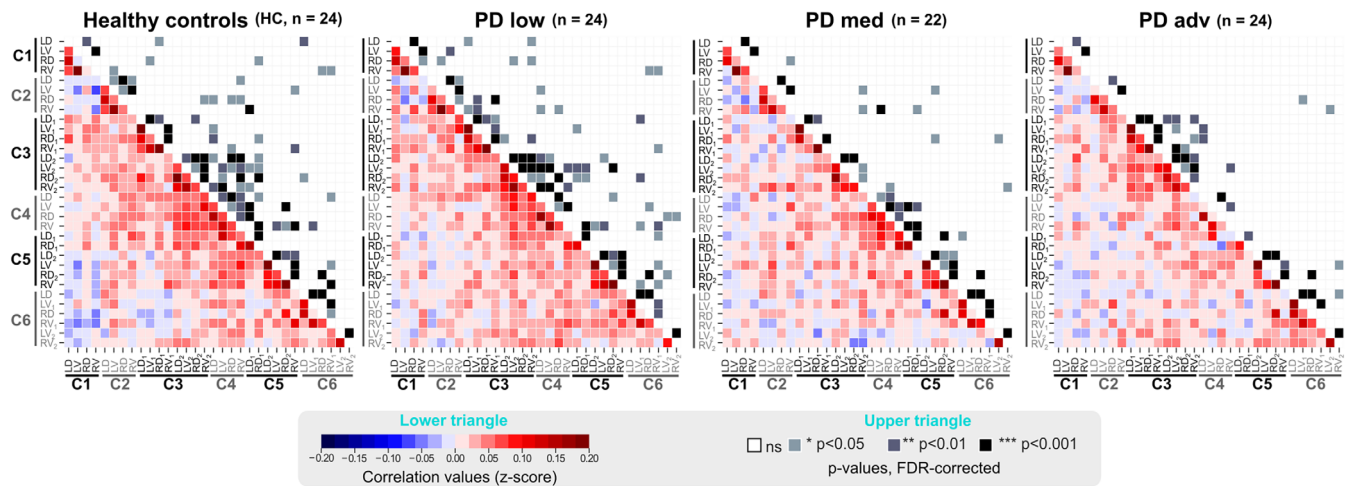


**FIG. 2.** Correlation matrices in each group. Lower triangle: the average of the Fisher's z-transformed scores reflecting the strength of the pairwise correlations between the 32 ROIs (regions of interest). Upper triangle: the mean of correlations that are significantly different from zero is highlighted in different shades of gray (FDR corrected for multiple comparison). [Color figure can be viewed at [wileyonlinelibrary.com](http://wileyonlinelibrary.com)]

85, PD<sub>med</sub>: 45, and PD<sub>adv</sub>: 40), indicating a weaker spinal FC with disease progression.

### Intersegmental FC

FC between ROIs located at different segmental levels (Fig. 3A) showed a significant decrease in the mean intersegmental correlation values across groups (Fig. 3B,  $t_{(93)} = -2.29$ ,  $P = 0.024$ ) but no age effect ( $t_{(93)} = -0.041$ ,  $P = 0.97$ ). A regression analysis conducted within the PD groups revealed a significant decrease in the upper-limb UPDRSIII scores (Fig. 3C, upper-UPDRSIII effect:  $t_{(69)} = -2.70$ ,  $P = 0.0085$ ; age effect:  $t_{(69)} = 0.82$ ,  $P = 0.41$ ) but not in the lower-limb UPDRSIII scores (lower-UPDRSIII effect:  $t_{(69)} = -0.58$ ,  $P = 0.56$ ; age effect:  $t_{(69)} = 0.03$ ,  $P = 0.97$ ).

The effect of distance in the rostro-caudal plane was tested statistically by fitting linear regressions in all groups with subjects as random effect (Fig. 3D). The analysis indicated that FC decreased linearly with spinal distance in all groups (HC:  $t_{(1200)} = -9.34$ ,  $P < 0.001$ ; PD<sub>low</sub>:  $t_{(1200)} = -7.32$ ,  $P < 0.001$ ; PD<sub>med</sub>:  $t_{(1100)} = -5.35$ ,  $P < 0.001$ ; PD<sub>adv</sub>:  $t_{(1200)} = -3.26$ ,  $P = 0.0011$ ), but no age effect was observed (HC:  $t_{(24)} = 0.83$ ,  $P = 0.42$ ; PD<sub>low</sub>:  $t_{(24)} = 1.24$ ,  $P = 0.22$ ; PD<sub>med</sub>:  $t_{(22)} = 1.23$ ,  $P = 0.23$ ; PD<sub>adv</sub>:  $t_{(24)} = -1.62$ ,  $P = 0.12$ ).

Further, we used a linear regression mixed model that included groups, distance, and age as fixed effects and subjects as a random effect. This model revealed a significant main effect of groups ( $\chi^2_{(3)} = 11.3$ ,  $P < 0.001$ ) and distance ( $\chi^2_{(1)} = 89.3$ ,  $P < 0.001$ ), as well as a significant interaction between groups and distance ( $\chi^2_{(3)} = 19.6$ ,  $P < 0.001$ ), but no age effect. More specifically, distance had a significant stronger effect (ie, stronger decrease in the FC with distance) on HC compared to both the PD<sub>med</sub> and PD<sub>adv</sub> (HC vs. PD<sub>med</sub>:

$t_{(4700)} = 2.82$ ,  $P < 0.0063$ ; HC vs. PD<sub>adv</sub>:  $t_{(4700)} = 4.30$ ,  $P < 0.001$ ), and no significant distance effect difference was observed between HC and PD<sub>low</sub> despite an apparent trend ( $t_{(4700)} = 1.66$ ,  $P = 0.096$ ).

We also observed significant difference between the PD<sub>low</sub> and PD<sub>adv</sub> groups ( $t_{(4700)} = 2.63$ ,  $P < 0.008$ ) in link with the effect of distance effect but not between PD<sub>low</sub> and PD<sub>med</sub> ( $t_{(4700)} = 1.10$ ,  $P = 0.27$ ), either PD<sub>med</sub> and PD<sub>adv</sub> ( $t_{(4700)} = 1.48$ ,  $P = 0.14$ ). In sum, these findings highlight the preservation of a distance-dependent intersegmental FC organization in PD patients, albeit diminished in the early stages of the disease.

FC between adjacent levels was then investigated by including  $z$ Corr between pairs of ROIs located in adjacent spinal levels in a mixed linear regression model with groups, adjacent-segments, and age as fixed effects and with subjects as a random effect (Fig. 4A). A significant main effect of groups ( $\chi^2_{(1)} = 3.86$ ,  $P < 0.049$ ) and adjacent-segments ( $\chi^2_{(4)} = 203.8$ ,  $P < 0.001$ , Fig. 4B) and a significant interaction between groups and adjacent-segments were observed ( $\chi^2_{(4)} = 20.24$ ,  $P < 0.001$ ) but no age effect ( $\chi^2_{(1)} = 0.018$ ,  $P = 0.89$ ). A subsequent regression analysis in the PD population revealed a significant decrease in the upper-limb UPDRSIII scores (Fig. 5C, upper-UPDRSIII effect:  $\chi^2_{(1)} = 7.60$ ,  $P < 0.0058$ ) and a significant effect of adjacent-segments ( $\chi^2_{(4)} = 96.56$ ,  $P < 0.001$ ) but no age effect ( $\chi^2_{(1)} = 0.84$ ,  $P = 0.35$ ). Yet when the lower-limb UPDRSIII scores were used in the model, no significant main effect of this factor was obtained (lower-UPDRSIII effect:  $\chi^2_{(1)} = 0.009$ ,  $P = 0.92$ ). Overall, the adjacent-segments' FC decreases across groups and is correlated with the upper-limb, but not the lower-limb, motor symptoms in PD patients.

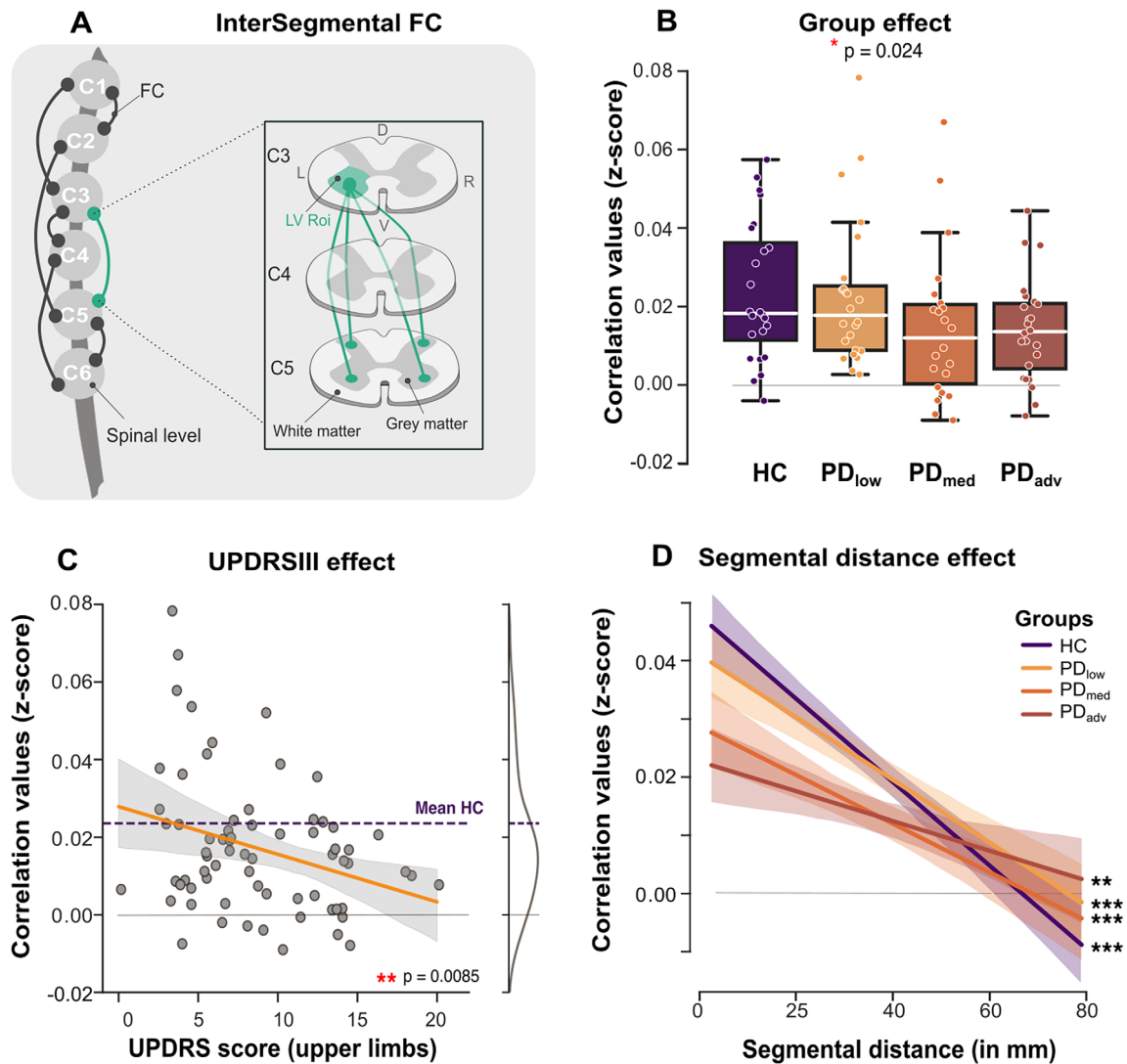


**FIG. 3.** Intersegmental functional connectivity. **(A)** Schematic representation of the intersegmental functional connectivity; the inset shows all possible intersegmental connections between the left-ventral horn (LV) at the C3 level and all the horns at the C5 level. **(B)** Boxplot of the average of z-scored correlation coefficients (z-Corr) extracted from the correlation matrices from each group (HC [healthy control], PD<sub>low</sub>, PD<sub>med</sub>, and PD<sub>adv</sub>). Each box represents the distribution (ie, from the 25th to the 75th percentile) of zCrr for each group, whereas the medians are represented by the horizontal white line inside the box. Black vertical lines denote the extreme values within a 1.5 interquartile range. **(C)** Regression analysis reflecting the relation between the upper-UPDRSIII (Unified Parkinson's Disease Rating Scale) scores and the mean zCrr in all PD patients (ie, all PD groups pooled together). Dots represent individual values, and the mean of the HC group is illustrated by a dash line and the 0 value by a gray line. The distribution of the mean zCrr (right y-axis) is represented by a continuous probability density curve. **(D)** Regression lines describing the relationship between the segmental distance (in mm) and the intersegmental zCrr in each group. \* $P < 0.05$ , \*\* $P < 0.01$ , and \*\*\* $P < 0.001$ . [Color figure can be viewed at [wileyonlinelibrary.com](https://onlinelibrary.wiley.com/terms-and-conditions)]

Then, we conducted mixed linear regression analyses for all possible adjacent segments in PD patients (Fig. 4D). In these five models, upper UPDRSIII, lower UPDRSIII, and age were considered as fixed effects, and subjects was considered as a random effect. Results showed that adjacent segmental FC decreased with upper-limb dysfunction, especially between segmental levels C4–C5 ( $t_{(69)} = -3.08$ ,  $P$ -corrected = 0.015) and C5–C6 ( $t_{(69)} = -2.73$ ,  $P$ -corrected = 0.020). However, no significant association was observed for lower-limb

UPDRSIII and FC between at any segmental levels (Supporting Data Tables S2 and S3).

### Intrasegmental FC

The intrasegmental analysis did not reveal any significant effect of groups (Fig. 5A,B,  $t_{(91)} = -0.87$ ,  $P = 0.38$ ) nor any main effect of age ( $t_{(91)} = 0.60$ ,  $P = 0.54$ ). Furthermore, the regression analysis of the PD groups only did not reveal significant changes in the

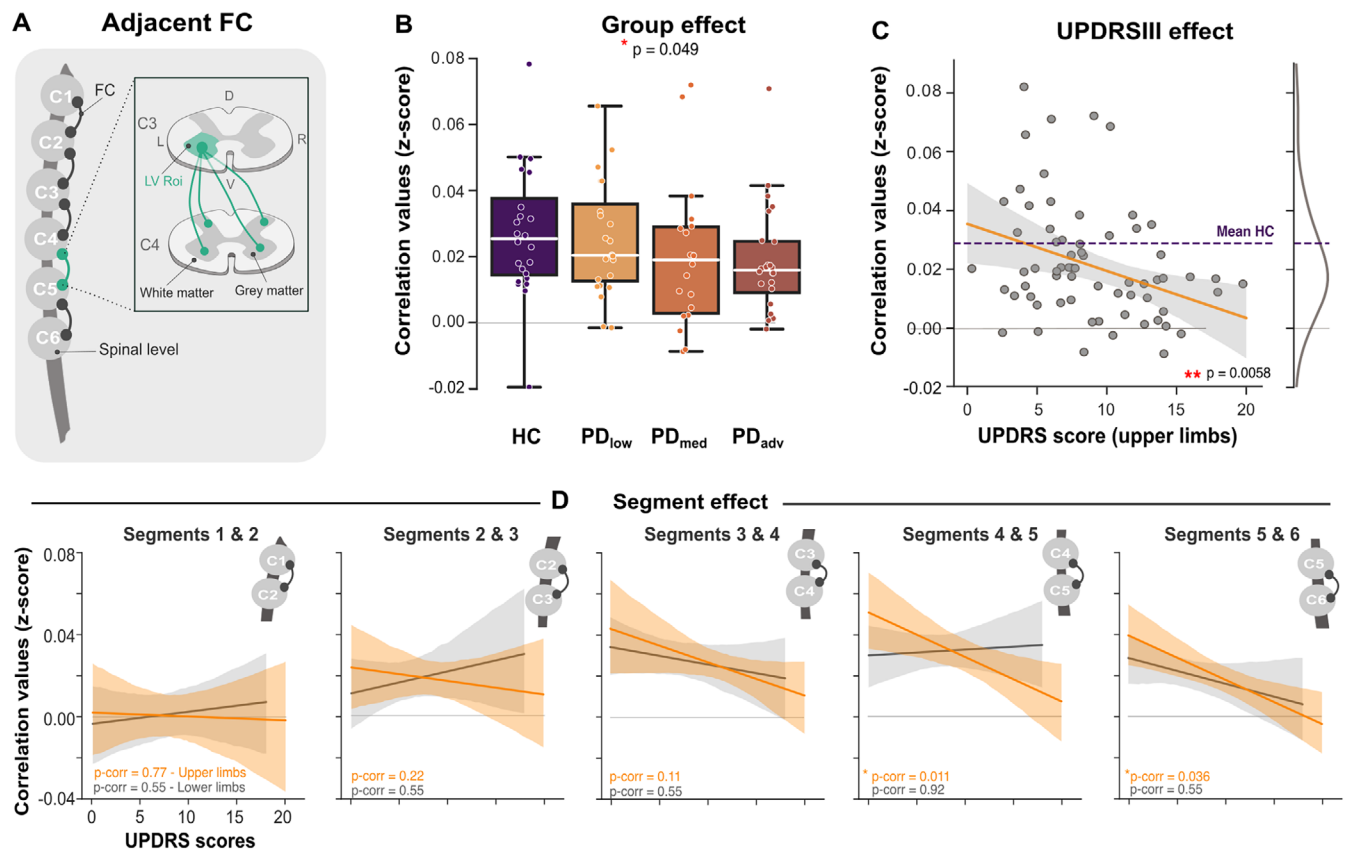


**FIG. 4.** Adjacent functional connectivity. **(A)** Schematic representation of the adjacent functional connectivity; the inset shows the FC (functional connectivity) between the left-ventral horn (LV) at the C3 level and all possible ROIs (regions of interest) located at the C4 adjacent level. **(B)** Boxplot of the average z-scored correlation (zCorr) reflecting the adjacent FC extracting the pairwise correlation matrices for each group (HC [healthy control], PD<sub>low</sub>, PD<sub>med</sub>, and PD<sub>adv</sub>). Each box represents the distribution (ie, from the 25th to the 75th percentile) of zCorr for each group, whereas the medians are represented by the horizontal white line inside the box. Black vertical extending lines denote the extreme values within a 1.5 interquartile range. **(C)** Regression analysis between the upper-UPDRSIII (Unified Parkinson's Disease Rating Scale) score and the mean zCorr in PD population (ie, all PD groups pooled together). Dots represent individual values, and the mean of the HC group is shown by a dash line and the 0 value by a gray line. The distribution of the mean zCorr (right y-axis) is represented by a continuous probability density curve. **(D)** Regression lines reflecting the relationship between the upper-UPDRSIII scores or the lower-UPDRSIII scores and the zCorr in PD patients for each of the five adjacent segments' connectivity; the *P*-values are FDR corrected for multiple comparisons. \* $P < 0.05$  and \*\* $P < 0.01$ . [Color figure can be viewed at [wileyonlinelibrary.com](http://wileyonlinelibrary.com)]

upper-limb UPDRSIII scores (Fig. 5C, upper-UPDRSIII effect:  $t_{(69)} = -1.27$ ,  $P = 0.21$ ; age effect:  $t_{(69)} = 1.27$ ,  $P = 0.20$ ) nor in the lower-limb UPDRSIII scores (lower-UPDRSIII effect:  $t_{(69)} = -0.27$ ,  $P = 0.78$ ; age effect:  $t_{(69)} = 0.88$ ,  $P = 0.38$ ).

## Discussion

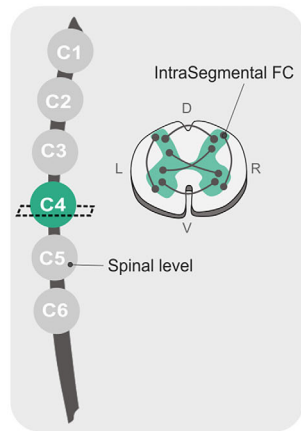
The present study provides the first evidence of FC changes in the cervical spinal cord in the groups of PD patients. ICA revealed that intrinsic spinal organization was reproducible across groups of HCs and PD patients. Yet the seed-to-seed analysis revealed a reduced segregation of spinal neural networks closely associated with PD progression. In addition, the average spinal FC decreases between segments were associated with the severity of upper-limb motor symptoms but not with that of the lower limbs. Thus, our results

shed new light on the characterization of the functional changes in the spinal cord during PD progression and may provide new perspectives for monitoring treatment approaches.

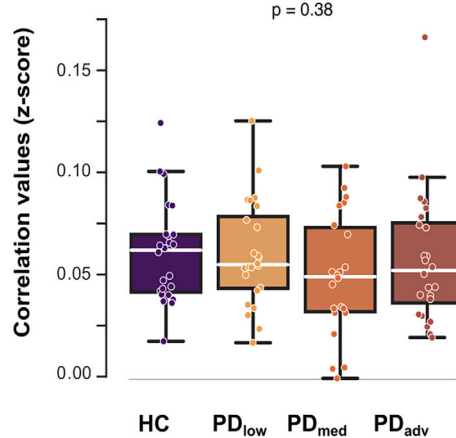
The spinal cord ICs obtained during rest presented spatially segregated patterns in both rostro-caudal and ventro-dorsal directions that strongly overlapped with the spinal-level probability maps,<sup>31</sup> therefore corroborating previous results.<sup>15,17,18</sup> These synchronous spinal networks overlap with corresponding dermatome or myotome serving different parts of the body.<sup>15,17,18</sup> Notably, these spinal networks were highly reproducible when the population was divided into four subgroups (HCs and PD patients at different stages), indicating that ICA allows for the identification of robust spinal networks in patient population and thus could provide a valuable tool for clinical application.

In line with previous studies, the seed-to-seed analysis revealed strong positive correlations mostly between

## A Intrasegmental FC



## B



## C

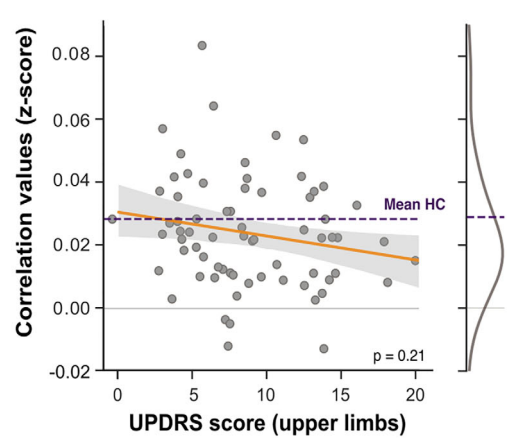


**FIG. 5.** Intrasegmental functional connectivity. **(A)** Schematic representation of the intrasegmental functional connectivity. **(B)** Boxplot of the z-scored correlation coefficients (zCorr) over the matrices for each group (HC [healthy control], PD<sub>low</sub>, PD<sub>med</sub>, and PD<sub>adv</sub>). Each box represents the distribution (ie, from the 25th to the 75th percentile) of zCorr for each group, whereas the medians are represented by the horizontal white line inside the box. Black vertical extending lines denote the extreme values within a 1.5 interquartile range. **(C)** Regression analysis between the upper-UPDRSIII (Unified Parkinson's Disease Rating Scale) score and the mean zCorr in PD patient population (ie, all PD groups pooled together). Dots represent individual values, and the mean of the HC group is shown by a dash line and the 0 value by a gray line. The distribution of the zCorr (right y-axis) is represented by a continuous probability density curve. D: dorsal, FC: functional connectivity, L: left, R: right, V: ventral. [Color figure can be viewed at [wileyonlinelibrary.com](http://wileyonlinelibrary.com)]

ROIs at the same spinal level<sup>15,17,18,32-34</sup> and negative correlations between long-distance segments. The distance-dependent organization along the rostro-caudal axis was supported by a linear decrease in FC from short- to long-distance segments in both HCs and PD patients. This follows key features of the spinal functional organization, in which two neighboring segments innervate two adjacent body parts whose function must be coordinated more strongly as compared to two more distant body parts.

It is interesting to note that the segregation of spinal networks with distance was progressively less pronounced in PD groups as compared to HCs. In addition, this decrease was significantly less pronounced in PD<sub>med</sub> and PD<sub>high</sub> groups as compared to the PD<sub>low</sub> group and HCs, indicating that disease severity may play a role in this regard. Such an effect has been reported by brain research studies revealing an increase in internetwork connectivity between distant networks involved in sensory and motor functions (putamen, cerebellum, and motor cortex<sup>35</sup>), as well as between distant networks such as subcortical and midbrain FC.<sup>36,37</sup> This loss of functional segregation may be interpreted as compensatory mechanism to maintain the integrity of the sensorimotor network due to the general reduction in FC observed in patients. Alternatively, it could reflect a decrease in selectivity of neural recruitment. Further investigations are needed to better understand these intersegmental FC changes with PD, including task-related fMRI and correlation between FC and sensorimotor performances.

Another prominent effect of PD at the spinal level was the absence of significant intrasegmental FC (within-network) differences, despite a significant decrease in intersegmental FC (internetworks) associated with upper-limb, but not lower-limb, motor symptoms. These findings highlight the progressive impairments in the spinal networks over PD progression and are in line with brain observations. For instance, PD-related changes between the different sensorimotor brain subnetworks (eg, superior parietal lobule and precentral, postcentral, and prefrontal areas) were found to be more pronounced than intranetwork FC changes.<sup>38</sup>

To help further confirm the localization of the intersegmental FC decrease, we considered the FC between adjacent segments. A significant decrease in FC was observed specifically between C4 and C5 as well as between C5 and C6 in association with motor symptom severity of the upper limbs but not the lower limbs. Interestingly, C4, C5, and C6 segments are predominantly activated during task-related MRI of the upper limbs<sup>20,21</sup> and are known to be related to the dermatomes and myotomes of these body areas. This finding suggests that the FC decrease between adjacent segments occurs specifically in segments involving upper-limb functions and are associated with motor symptom severity in this body part.

Some limitations should be acknowledged; indeed clinical manifestation varies from patient to patient. Although we have tried to consider what we believe to be the most important cofactors (age, sex, and



lateralization of the disease), it would be obviously desirable in the future to test the effect of other within-subject heterogeneities (medication, affected limbs, non-motor symptoms, etc.). In addition, future works may further confirm the specificity of spinal FC changes by examining whether this relationship can also be found between lower-limb motor symptoms and FC changes in lower spinal levels.

Overall, we provide the first evidence of PD-related dysfunction of the sensorimotor pathways at the spinal level corroborating the alteration of sensory and motor regions at the brain level along the corticostriatal pathway. In this study, we focused on spinal cord rsfMRI data to characterize better the spinal FC in PD relative to their healthy counterparts. The logical next step for future studies would be to investigate PD-related FC changes across multiple levels. Our group is currently developing new pipelines to process and analyze the brain and cervical spinal cord fMRI data acquired simultaneously in this data set, which would provide insights into the effect of PD at the central nervous system level as a whole.<sup>16,23</sup>

Investigation of dorsal spinal cord stimulation therapy in PD patients has recently increased, showing that this approach can improve pain and motor symptoms,<sup>39</sup> although the underlying neurophysiological mechanisms are not yet clear. Interestingly, this therapeutic approach has been used successfully as salvage therapy in a subgroup of PD patients where dopamine treatment and deep brain stimulation were no longer effective.<sup>40</sup> The results of the current study suggest the possibility that spinal rsfMRI can be used as a tool to determine whether the action mechanisms of dorsal spinal cord stimulation are based on the restoration of FC between various spinal segments. This latter point is especially relevant because our results demonstrate specificity between upper-limb motor symptom severity and the spinal segments that innervate this body part.

Finally, the present study provides supporting evidence that spinal cord fMRI can serve as a powerful tool to characterize, in vivo, spinal circuits for a variety of neurological diseases and a practical guide on how to implement it. ■

**Acknowledgments:** We thank the Clinical, Biospecimen, Imaging & Genetic (C-BIG) repository for help in participant recruitment and the brain imaging centre of The Neuro for help in data acquisition. We thank all participants involved in this study.

### Data Availability Statement

The data and pipelines that support the findings of this study are available from the corresponding author, upon reasonable request. A repository with spinal cord

preprocessing pipeline is available here: [https://github.com/CarolineLndl/BMPD\\_SC\\_fmri\\_landelle-et-al](https://github.com/CarolineLndl/BMPD_SC_fmri_landelle-et-al).

## References

1. Jellinger KA. Neuropathology of sporadic Parkinson's disease: evaluation and changes of concepts: neuropathology of sporadic PD. *Mov Disord* 2012;27:8–30.
2. Rahayel S, Mišić B, Zheng Y-Q, Liu Z-Q, Abdelgawad A, Abbasi N, et al. Differentially targeted seeding reveals unique pathological alpha-synuclein propagation patterns. *Brain* 2022;145:1743–1756.
3. Del Tredici K, Braak H. Spinal cord lesions in sporadic Parkinson's disease. *Acta Neuropathol* 2012;124:643–664.
4. Del Tredici K, Braak H. Review: sporadic Parkinson's disease: development and distribution of  $\alpha$ -synuclein pathology. *Neuropathol Appl Neurobiol* 2016;42:33–50.
5. Horsager J, Andersen KB, Knudsen K, Skjærbæk C, Fedorova TD, Okkels N, et al. Brain-first versus body-first Parkinson's disease: a multimodal imaging case-control study. *Brain* 2020;143:3077–3088.
6. Nardone R, Höller Y, Brigo F, Versace V, Sebastianelli L, Florea C, et al. Spinal cord involvement in Lewy body-related  $\alpha$ -synucleinopathies. *J Spinal Cord Med* 2020;43:832–845.
7. Raudino F, Leva S. Involvement of the spinal cord in Parkinson's disease. *Int J Neurosci* 2012;122:1–8.
8. Buchman AS, Nag S, Leurgans SE, Miller J, VanderHorst VGJM, Bennett DA, et al. Spinal Lewy body pathology in older adults without an antemortem diagnosis of Parkinson's disease: spinal lewy bodies in older adults. *Brain Pathol* 2018;28:560–568.
9. Oinas M, Paetau A, Myllykangas L, Norkola I-L, Kalimo H, Polvikoski T.  $\alpha$ -Synuclein pathology in the spinal cord autonomic nuclei associates with  $\alpha$ -synuclein pathology in the brain: a population-based Vantaa 85+ study. *Acta Neuropathol* 2010;119:715–722.
10. Beach TG, Adler CH, Sue LI, Vedders L, Lue L, White Iii CL, et al. Multi-organ distribution of phosphorylated alpha-synuclein histopathology in subjects with Lewy body disorders. *Acta Neuropathol* 2010;119:689–702.
11. Bloch A, Probst A, Bissig H, Adams H, Tolnay M. alpha-Synuclein pathology of the spinal and peripheral autonomic nervous system in neurologically unimpaired elderly subjects. *Neuropathol Appl Neurobiol* 2006;32:284–295.
12. Braak H, Sastre M, Bohl JRE, de Vos RAI, Del Tredici K. Parkinson's disease: lesions in dorsal horn layer I, involvement of parasympathetic and sympathetic pre- and postganglionic neurons. *Acta Neuropathol* 2007;113:421–429.
13. Sumikura H, Takao M, Hatsuta H, Ito S, Nakano Y, Uchino A, et al. Distribution of  $\alpha$ -synuclein in the spinal cord and dorsal root ganglia in an autopsy cohort of elderly persons. *Acta Neuropathol Commun* 2015;3:57.
14. Samantaray S, Knaryan VH, Shields DC, Banik NL. Critical role of calpain in spinal cord degeneration in Parkinson's disease. *J Neurochem* 2013;127:880–890.
15. Barry RL, Smith SA, Dula AN, Gore JC. Resting state functional connectivity in the human spinal cord. *eLife* 2014;3:e02812.
16. Khatibi A, Vahdat S, Lungu O, Finsterbusch J, Büchel C, Cohen-Adad J, et al. Brain-spinal cord interaction in long-term motor sequence learning in human: an fMRI study. *Neuroimage* 2022;253:119111.
17. Kinany N, Pirondini E, Micera S, Van De Ville D. Dynamic functional connectivity of resting-state spinal cord fMRI reveals fine-grained intrinsic architecture. *Neuron* 2020;108:424–435.e4.
18. Kong Y, Eippert F, Beckmann CF, Andersson J, Finsterbusch J, Büchel C, et al. Intrinsically organized resting state networks in the human spinal cord. *Proc Natl Acad Sci U S A* 2014;111:18067–18072.
19. Vahdat S, Khatibi A, Lungu O, Finsterbusch J, Büchel C, Cohen-Adad J, et al. Resting-state brain and spinal cord networks in humans are functionally integrated. *PLoS Biol* 2020;18:e3000789.

20. Kinany N, Pirondini E, Micera S, Van De Ville D. Spinal cord fMRI: a new window into the central nervous system. *Neuroscientist* 2022. <https://doi.org/10.1177/10738584221101827>
21. Landelle C, Lungu O, Vahdat S, Kavounoudias A, Marchand-Pauvert V, De Leener B, et al. Investigating the human spinal sensorimotor pathways through functional magnetic resonance imaging. *Neuroimage* 2021;245:118684.
22. Tinnermann A, Büchel C, Cohen-Adad J. Cortico-spinal imaging to study pain. *Neuroimage* 2020;224:117439.
23. Vahdat S, Lungu O, Cohen-Adad J, Marchand-Pauvert V, Benali H, Doyon J. Simultaneous brain-cervical cord fMRI reveals intrinsic spinal cord plasticity during motor sequence learning. *PLoS Biol* 2015;13:e1002186.
24. Movement Disorder Society Task Force on Rating Scales for Parkinson's Disease. The unified Parkinson's disease rating scale (UPDRS): status and recommendations. *Mov Disord* 2003;18:738–750.
25. Maehara M, Ikeda K, Kurokawa H, Ohmura N, Ikeda S, Hirokawa Y, et al. Diffusion-weighted echo-planar imaging of the head and neck using 3-T MRI: investigation into the usefulness of liquid perfluorocarbon pads and choice of optimal fat suppression method. *Magn Reson Imaging* 2014;32:440–445.
26. Cohen-Adad J, Alonso-Ortiz E, Abramovic M, Arneitz C, Atcheson N, Barlow L, et al. Generic acquisition protocol for quantitative MRI of the spinal cord. *Nat Protoc* 2021;16:4611–4632.
27. De Leener B, Levy S, Dupont SM, Fonov VS, Stikov N, Louis Collins D, et al. SCT: spinal cord toolbox, an open-source software for processing spinal cord MRI data. *Neuroimage* 2017;145:24–43.
28. Kasper L, Bollmann S, Diaconescu AO, Hutton C, Heinzle J, Iglesias S, et al. The PhysIO toolbox for modeling physiological noise in fMRI data. *J Neurosci Methods* 2017;276:56–72.
29. Varoquaux G, Sadaghiani S, Pinel P, Kleinschmidt A, Poline JB, Thirion B. A group model for stable multi-subject ICA on fMRI datasets. *Neuroimage* 2010;51:288–299.
30. Abraham A, Pedregosa F, Eickenberg M, Gervais P, Mueller A, Kossaifi J, et al. Machine learning for neuroimaging with scikit-learn. *Front Neuroinform* 2014;8:14. <https://doi.org/10.3389/fninf.2014.00014/abstract>
31. Cadotte DW, Cadotte A, Cohen-Adad J, Fleet D, Livne M, Wilson JR, et al. Characterizing the location of spinal and vertebral levels in the human cervical spinal cord. *Am J Neuroradiol* 2015;36:803–810.
32. Eippert F, Kong Y, Winkler AM, Andersson JL, Finsterbusch J, Büchel C, et al. Investigating resting-state functional connectivity in the cervical spinal cord at 3 T. *Neuroimage* 2017;147:589–601.
33. Liu X, Zhou F, Li X, Qian W, Cui J, Zhou IY, et al. Organization of the intrinsic functional network in the cervical spinal cord: a resting state functional MRI study. *Neuroscience* 2016;336:30–38.
34. Weber KA, Sentis AI, Bernadel-Huey ON, Chen Y, Wang X, Parrish TB, et al. Thermal stimulation alters cervical spinal cord functional connectivity in humans. *Neuroscience* 2018;369:40–50.
35. Simioni AC, Dagher A, Fellows LK. Compensatory striatal-cerebellar connectivity in mild-moderate Parkinson's disease. *Neuroimage* 2016;10:54–62.
36. Hacker CD, Perlmuter JS, Criswell SR, Ances BM, Snyder AZ. Resting state functional connectivity of the striatum in Parkinson's disease. *Brain* 2012;135:3699–3711.
37. Manza P, Zhang S, Li C-SR, Leung H-C. Resting-state functional connectivity of the striatum in early-stage Parkinson's disease: cognitive decline and motor symptomatology: striatal connectivity in Parkinson's disease. *Hum Brain Mapp* 2016;37:648–662.
38. Caspers J, Rubbert C, Eickhoff SB, Hoffstaedter F, Südmeyer M, Hartmann CJ, et al. Within- and across-network alterations of the sensorimotor network in Parkinson's disease. *Neuroradiology* 2021;63:2073–2085.
39. Cai Y, Reddy RD, Varshney V, Chakravarthy KV. Spinal cord stimulation in Parkinson's disease: a review of the preclinical and clinical data and future prospects. *Bioelectron Med* 2020;6:5.
40. Pinto de Souza C, Hamani C, Oliveira Souza C, Lopez Contreras WO, dos Santos Ghilardi MG, Cury RG, et al. Spinal cord stimulation improves gait in patients with Parkinson's disease previously treated with deep brain stimulation: spinal cord stimulation in PD. *Mov Disord* 2017;32:278–282.

## Supporting Data

Additional Supporting Information may be found in the online version of this article at the publisher's web-site.

# SGML and CITI Use Only DO NOT PRINT

## Author Roles

C.L., L.S.D., O.L., B.L., J.D.: conception and design of the study and methods

C.L., L.S.D., O.L., B.L.: acquisition

C.L., B.L., O.L., B.M.: data analysis

C.L., O.L., J.D.: writing of the original draft

C.L., O.L., B.M., B.L., J.D.: writing—review and editing

## Full financial disclosures for the previous 12 months

C.L: has received post-doctoral fellowship from the FRQS (“Fédération de recherche du Québec – Santé”) and has received travel support from QBIN (Quebec Bio-Imaging Network); L.S.D: has no financial disclosures.; O.L: has no financial disclosures.; B.M: has received grant support from the Canadian Institutes of Research (CIHR), Natural Sciences and Engineering Research Council of Canada (NSERC), Canada Research Chairs, Healthy Brain for Healthy Lives (HBHL), Michael J. Fox and Brain Canada.

B.L: has no financial disclosures.; J.D: has received grant support from the Natural Sciences and Engineering Research Council of Canada (NSERC, Grant No. 248074); Brain Canada Platform (Grant No. 255934) and Healthy Brain for Healthy Lives (HBHL, Grant No. 247363).